Sorting of Brownian particles by the pulsed application of an asymmetric potential

L. Gorre-Talini, S. Jeanjean, and P. Silberzan*
Laboratoire de Physico-Chimie Curie, UMR CNRS/IC 168, Institut Curie, Section de Recherche-11, rue Pierre et Marie Curie, 75231 Paris Cédex 05, France
(Received 19 February 1997)

We submit a suspension of Brownian latex spheres in water to a spatially periodic and asymmetric potential successively switched on and off. Such a potential is created by dielectrophoretically induced forces resulting from the application of a high-frequency electric field between a plane electrode and a blazed optical grating. As expected, we observe a net macroscopic drift of the particles. Their average velocities have been measured as a function of the time during which the field is switched off. We observe a quantitative agreement with the theoretical predictions. In particular, the velocities strongly differ according to the size of the latex spheres, which should open the way to devices aimed at the separation of micrometer and submicrometer particles. The geometry of the gratings as well as the concentration and the surface functions of the particles has also been investigated. [S1063-651X(97)14808-5]

PACS number(s): 05.40.+j, 82.45.+z, 82.70.Dd

INTRODUCTION AND THEORETICAL BASIS

On the way towards the understanding of biological motors, a large theoretical effort has come to the conclusion that a macroscopic directed motion can exist even without any macroscopic field or gradient [1–6]. Only two ingredients are then necessary to get such a ''force-free'' motion: namely, dissipation and a local asymmetry of the energetic potential the object of interest is submitted to.

The sphere of application of these concepts being wider than the biological molecular motor problem, we will rather focus on their relevance in the design of separation devices in this paper. This idea, which was originally proposed in Ref. [1], has already received some experimental support. One of its most interesting features is its very high versatility, which should make it suitable for micrometer size biological objects such as very long DNA molecules, viruses, chromosomes, etc. Indeed, separations of these objects are widely reported to be very slow processes with a poor efficiency, whereas their importance, for instance in the human genome project, has received increasing attention.

Let us concentrate on a simple system in which Brownian particles are submitted to a low-symmetry energetic potential such as the one depicted in Fig. 1. This potential is successively switched on and off [1]. We note $a+b$, the period of the potential, and $a/(a+b)$, its asymmetry $(a<b)$. Its amplitude E is supposed to be far larger than the thermal energy kT.

When the potential is ''on,'' the particles are trapped in positions corresponding to the minima of this potential. As soon as it is switched off, they diffuse and, if one waits long enough, they can diffuse over distances larger than a or b. When the field is switched on again, a certain fraction of these particles will then fall in the trap next to the one previously occupied. As the system of traps is of low symmetry, more particles are going to drift to the right than to the left using the conventions of direction of Fig. 1. By repeating this process a large number of times, one can get a macroscopic motion even though there is no macroscopic gradient of any kind in this description (which justifies the term force-free motion). Moreover, the average macroscopic velocity of the particles is conditioned by the diffusive step which takes place when the field is switched off. Hence particles of different sizes (different diffusion coefficients) will not move at the same velocity and will therefore be separated.

As a matter of fact, a simple calculation drawn from the classic diffusion equations yields [1]

$$p_f=\frac{1}{2}\,\mathrm{erfc}\left(\frac{a}{\sqrt{4Dt_{\mathrm{off}}}}\right), \tag{1}$$

$$p_b=\frac{1}{2}\,\mathrm{erfc}\left(\frac{b}{\sqrt{4Dt_{\mathrm{off}}}}\right), \tag{2}$$

where p_f and p_b are, respectively, the probability of going forward (to the right in Fig. 1) and backward (to the left in Fig. 1), D is the diffusion coefficient, and t_{off} the time during which the potential is switched off. The macroscopic drift is thus expected to vary exponentially with the diffusion coefficient, which obviously is very promising for separating particles differing in sizes.

Along these lines, several groups have started experiments using these concepts on model particles. In one of these experiments, a single particle was optically trapped in a structure presenting the necessary geometrical characteristics

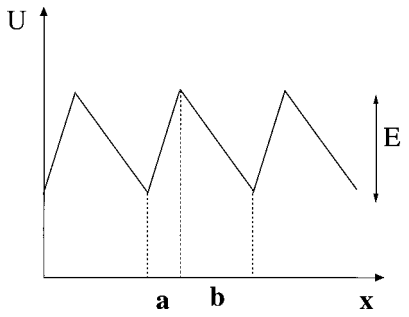

FIG. 1. Periodic asymmetric energetic potential as a function of the spatial coordinate x and characterized by the lengths a and b.

[7]. In that case the observed drift was qualitatively well described by the above description. However, only one particle could be handled at the time, which made the setup impracticable for separation purposes. For experiments dealing with many spheres, two-dimensional (2D) electrodes sputtered on glass using microlithography techniques were used [8,9]. The design of these electrodes was such that an efficient trapping of the particles was possible by using the dielectrophoretic effect. The main features of the theoretical predictions were observed, and in particular the particles were observed to drift in the expected direction, their macroscopic velocities depending on their sizes in a way qualitatively described by the simple model just exposed. However, several problems were encountered by these authors. First, in some cases, a large sticking of the particles made the measurements not practicable after a few minutes, and second, even when this sticking was not so problematic, an instability due to charge injection [10] and depending on the frequency of the electric field was noted. In Ref. [9], heavy particles of large dielectric constants (silica particles) had to be used so that their weight confined them to the vicinity of the electrodes and they could be efficiently trapped using a negative dielectrophoretic effect. Experimental results were in good agreement with the expected behaviors, although no backward motion was observed and an adjustable geometrical parameter, difficult to control in those particular designs, had to be plugged into the theoretical equations to interpret the experiments. However, in practical situations, the density of the objects to be separated is not very high *a priori* and a more versatile device would be welcome.

In this paper, we present a new system in which trapping is more efficient and we demonstrate its applicability to much lighter polystyrene spheres of various sizes and various surface functions.

PRINCIPLE OF THE EXPERIMENTS

As in Refs. [8] and [9], we have chosen to use the dielectrophoretic effect to trap the particles. However, instead of using 2D evaporated electrodes, we have used an electrode whose surface relief itself presents the necessary geometrical characteristics [Fig. 2(a)]. This ''factory roof'' shape can be found commercially as blazed diffraction gratings (see experimental section).

The other electrode is a plane and we apply an ac electric field between the two. As a result of the surface morphology, this field is not uniform (much stronger on the ridges) and, depending on the frequency of the electric field and on the contrast of polarizabilities between the particles and the surrounding medium, one expects the particles to be trapped on the ridges (positive dielectrophoresis) or in the valleys where the field is of lower intensity (negative dielectrophoresis). In any case the energetic potentials obtained with such a device have the desired properties of asymmetry and periodicity (see preliminary experiments).

EXPERIMENTAL SETUP

As already mentioned, we have used blazed diffraction gratings as one of our electrodes. A diffraction grating is an optical component which is the key part of most spectrometers. In some applications of these gratings, it is important to minimize the diffracted intensity at the zeroth order, and a convenient way of doing that is to give them the peculiar ''factory roof'' shape shown in Fig. 2(a) (blazed gratings). Their geometrical characteristics are then optimized, for a particular range of wavelength, in order to get the maximum power at a given order of diffraction. They are thus commercially available in a variety of periods and asymmetries.

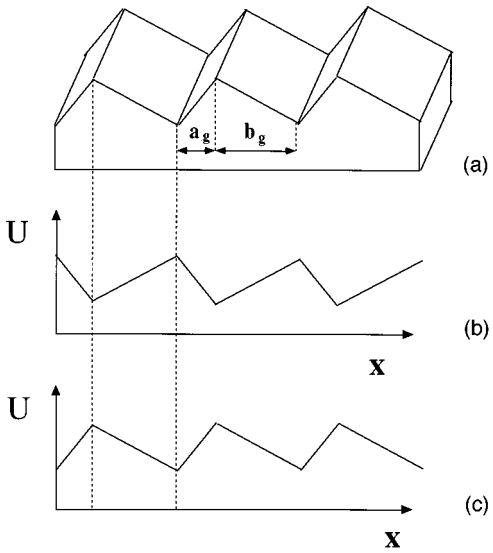

FIG. 2. Schematic representation of the surface of a diffraction grating (a) and approximations of the energetic potentials experienced by the particles in the regime of positive dielectrophoresis (b) and negative dielectrophoresis (c).

The experimental results we present in this paper are obtained with aluminum-coated infrared gratings of either 300 or 150 grooves per mm (i.e., periods of 3.33 or 6.67 μm) (Optometrics USA, Ayer, MA). We note a_g and b_g, the lengths of the small side and the large side of the periodical pattern (a_g+b_g being the period itself) [see Fig. 2(a)], and we define $x_g=a_g/(a_g+b_g)$ as the asymmetry ratio (here the index g stands for geometrical). In the following we will refer to each grating by its number of grooves per mm and its asymmetry (the grating 150/0.16 has thus 150 grooves per mm and a ratio $x_g=0.16$). For the sake of clarity, the lengths a_g and b_g of each grating are listed in Table I.

Since the particles we use are charged, they tend to be attracted to the metallic surface by an electric mirror effect. They then stick irreversibly to it. The surfaces of the gratings have therefore to be treated by a porous material which would be transparent from an electric point of view, but which would prevent this irreversible adsorption. For that purpose, we use a porous silica film. This is done by spin

TABLE I. Characteristics of the diffraction gratings used in the experiments. a_g and b_g are the characteristic geometrical lengths in the plane, and h is the height between the ridges and the valleys.

	Grating 150/0.16	Grating 150/0.09	Grating 300/0.36
a_g (μm)	1.1	0.6	1.2
b_g (μm)	5.57	6.07	2.13
h (μm)	2.47	1.91	1.6

coating directly onto the grating surface a silicate solution [9] (SilicaFilm from Emulsitone, Whippany, NJ), which we let polymerize just enough to get some mechanical strength without getting to the point where the film is too good an insulator.

The other electrode is a glass lamella coated with a conductive layer of ITO [$\rho = 20\ \Omega$/square (ICMC, France)].

All electrical connections are performed with silver paint and reinforced in a second time with epoxy.

In some of the experiments, the attenuation in the applied ac. voltage due to the quite high capacitance of the cell formed by the sandwich grating/water/ITO slide is too high. In these cases, we removed the ITO layer on all the surface of the slide, but on a narrow strip along its length. This is performed electrochemically with nail polish to protect the part to be left conductive.

The particles dealt with in this study are polystyrene fluorescent latex spheres (Molecular Probes, Eugene, OR) of diameters ranging between 10 nm and 2.5 μm. To avoid aggregation, their surface is functionalized. We have mainly used carboxylate-modified (CM) latex beads, but also sulfate, aldehyde sulfate, carboxyl, and amine modified beads. In the experimental conditions experienced here, all these surface groups are dissociated. Unless otherwise specified, experiments reported in the following deal with CM latex beads. A suspension of these spheres is then diluted in ultrapure water to a concentration of the order of 10^{-2}%, deposited on the grating and covered up by the ITO slide. The cell is then sealed with vacuum grease or sealing paste to a thickness of the order of 20 μm.

The electrodes are connected to a function synthetizor (Philips, PM 5193), itself switched successively on and off by a PC equipped with a I/O board (Keithley). Practically, the amplitude of the ac voltage varies from 10 to 20 V peak to peak and its frequency from 1 kHz to 50 MHz. Frequencies lower than 1 kHz were not explored to avoid electrolysis of water. The residual dc contribution of the field was successfully eliminated by a 100-nF capacitance.

The cell is placed on the stage of a microscope, and the movements of the individual particles are observed by fluorescence microscopy. The time sequences are recorded on a VCR for further analysis.

The analysis then proceeds as follows: We count the displacement of several particles over several time cycles such as to obtain about 100 displacements for a given t_{off}. Probabilities can then be calculated from these data. If N is the total number of displacements, we call N_{+i} the number of displacements from one trap to the ith trap in the forward direction (to the right in Fig. 1) and N_{-i} in the backward direction. The probability for a particle to move a distance of i periods during a time cycle is then $p_{\pm i} = N_{\pm i}/N$. During some of the experiments, the time t_{off} was long enough to observe displacements over up to three periods.

The probability of going forward is then $p_f = \Sigma_{i=1}^{\infty} p_{+i}$, the probability of going backward being $p_b = \Sigma_{i=1}^{\infty} p_{-i}$.

PRELIMINARY EXPERIMENTS: TRAPPING AND DIFFUSION COEFFICIENT

When the voltage is on, the particles are trapped within a fraction of a second on lines parallel to the grooves of the grating. When the cell has just been sealed, trapping occurs on the ridges of the grating, which are the regions of maximum field intensity, showing that positive dielectrophoresis of the particles is involved. The trapping is then effective within a wide range of frequencies (from 1 kHz to 5 MHz) and is strong enough to trap particles of diameter as small as 10 nm. No trapping occurs at frequencies larger than 5 MHz.

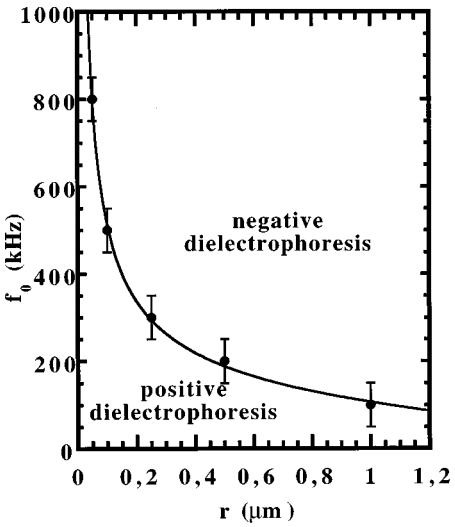

FIG. 3. Crossover frequency from positive to negative dielectrophoresis as a function of the radius r of the CM latex beads. The solid line represents the fit of the experimental values following Eq. (A5).

A few minutes later, the behavior of the particles is modified: While they are still trapped on the ridges at low frequencies, they are attracted to the hollows at higher frequencies. We attribute this behavior to an increase of the salinity of the solution due to ions of vacuum grease diffusing into the cell. Increasing the concentration of ions in the solution actually tends to increase the dielectric constant of the electrolyte, which becomes larger than that of the particles at high frequencies. The particles are then attracted to the regions of minimum field intensity (negative dielectrophoresis). We have observed no further evolution of the trapping during the time of experiment (up to 1 h). Trapping of colloidal particles in the regimes of positive and negative dielectrophoresis has been studied by several authors [9,11,12].

In the case of positive dielectrophoresis, the energetic potential experienced by the beads has thus the characteristics of the mirror of the surface relief [Fig. 2(b)], whereas in the case of negative dielectrophoresis it has the same characteristics as the grating itself [Fig. 2(c)]. In the following part, we shall come back in more details to a more precise determination of the mapping of the electric field.

The frequency f_0 at which the cross over from positive to negative dielectrophoresis occurs depends on the size of the particles: The smaller the particles, the larger the frequency. The plot of the cross over frequency as a function of the radius of the latex spheres is shown in Fig. 3. The solid curve delimits two domains: on its right negative dielectrophoresis, on its left positive dielectrophoresis. The qualitative interpretation of the variations of f_0 with the size of the particles is detailed in the Appendix.

Once the salinity of the solution is increased, we observe

that in the case of positive dielectrophoresis the dielectrophoretic force gives rise to instabilities in the bulk of the solution. As soon as the field is applied, a strong and directed flow occurs. This flow is always directed to the right in Fig. 2(a) near the surface of the grating and is strong enough to carry trapped particles away. This pumping effect may be due to thermal gradients induced by the local heating of the electrolyte in the regions of maximum field intensity [13]. Its study is beyond the scope of this paper and will be detailed in a forthcoming publication.

The presence of these instabilities hinders the proper achievement of trapping and detrapping cycles. As we also need to correctly seal the cell in order to avoid any leak, we have performed most of the experiments at high frequencies for which the particles are trapped in the regions of minimum field intensity. As shown in the following, we have nevertheless checked that the location of trapping does not change the characteristics of motion. Practically, negative dielectrophoresis experiments were performed with an ac field at a frequency of 1 MHz and an amplitude peak to peak of 20 V. As a result of the finite value of the capacitance of our experimental cell, this yields an effective voltage between the electrodes of approximately 10 V. The time during which the ac voltage is applied is systematically set at $t_{on}=3$ s, which is long enough to ensure an efficient trapping of all the studied particles.

In order to compare our results with Eqs. (1) and (2), we have measured the diffusion coefficients of 0.5 and 1-μm particles on the surface of each grating. The results are in agreement with the Stokes-Einstein formula $D=kT/6\pi\eta R$ within 10%. The cell being thick enough, no effect due to diffusion close to the walls appear as in Refs. [8] and [9]. In particular, no significant or systematic differences between the diffusion coefficients D_x and D_y in the x and y directions are observed, showing that the roughness of the surface does not induce nonisotropic diffusion behaviors.

DISTRIBUTION OF THE FIELD INTENSITY

As the energetic potential experienced by the beads is proportional to the squared intensity of the electric field (see the Appendix), only a detailed analysis of the distribution of the field intensity can give a correct description of the shape of the potential and the exact position of its maxima and minima. We have therefore numerically calculated the electrostatic potential between the electrodes. The principle of the relaxation method described in Ref. [14] consists in ruling the plane in small squares of approximate size 0.1 μm, the value of the potential at each point M_0 being determined by the values of the potential at the four points M_1, M_2, M_3, and M_4, surrounding M_0. One can actually show that the value of the potential at the point M_0 is given by

$$V_0=\frac{V_1+V_2+V_3+V_4}{4}. \tag{3}$$

A zero potential is first attributed to all the points between the electrodes, whereas a given potential is imposed on the electrodes. The potential at each point is then calculated using Eq. (3), and after about 1000 iterations the values of the potential remain constant. The intensity of the electric field

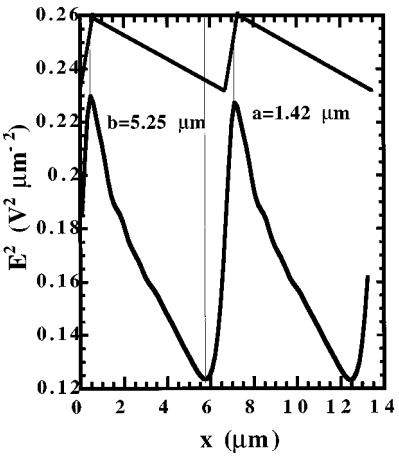

FIG. 4. Shape of the energetic potential experienced by the beads. This curve is obtained by computing the squared intensity E^2 of the electric field as a function of the spatial coordinate x created 3 μm above the surface of the grating 150/0.09 with 10 V between the grating and the ITO slide. The two electrodes are separated by 20 μm. The corresponding shape of the surface of the grating is shown above the curve.

$$E=\sqrt{\left(\frac{\partial V}{\partial x}\right)^2+\left(\frac{\partial V}{\partial y}\right)^2}$$

at a given height of the surface of the grating is then computed.

Figure 4 shows an example of the plot of E^2 as a function of the distance x and the corresponding surface of the grating for the grating 150/0.09. From such a plot one can easily determine the lengths a and b characterizing the energetic potential in the case of positive or negative dielectrophoresis. The plot of Fig. 4 shows that the maximum and minimum of the potential do not exactly correspond to the geometric features of the grating, and in this case, the lengths a and b corresponding to the energetic potential are fairly different from a_g and b_g as $a=1.42$ μm and $a_g=0.6$ μm. The results obtained for the three gratings are listed in Table II.

In the following, the lengths a and b we refer to are indeed the computed lengths of the energetic potential. By performing this calculation at different levels between the plate and grating, one can show that the level at which the field is either minimum or maximum is on the grating surface itself. This situation is very different from geometries using two-dimensional electrodes sputtered on an insulator [8,9]. In this latter case, the region of minimum field was as far as possible from the plane of the electrodes, and hence only heavy particles (silica spheres) could be used in the negative dielectrophoretic regime so that gravity confined

TABLE II. Characteristic lengths a and b and asymmetry ratio $x=a/(a+b)$ of the energetic potential derived from the calculation of the field intensity created on the surface of each grating.

	Grating 150/0.16	Grating 150/0.09	Grating 300/0.36
a (μm)	1.58 ± 0.08	1.42 ± 0.08	1.13 ± 0.07
b (μm)	5.09 ± 0.08	5.25 ± 0.08	2.20 ± 0.07
x	0.24	0.21	0.34

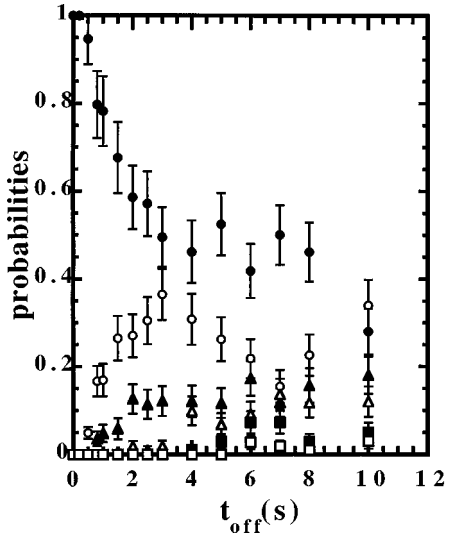

FIG. 5. Probabilities p_0 (solid circles), p_{+1} (open circles), p_{-1} (solid triangles), p_{+2} (open triangles), p_{-2} (solid squares), and p_{+3} (open squares) as a function of t_{off} for 0.5-μm CM latex beads on the grating 300/0.36.

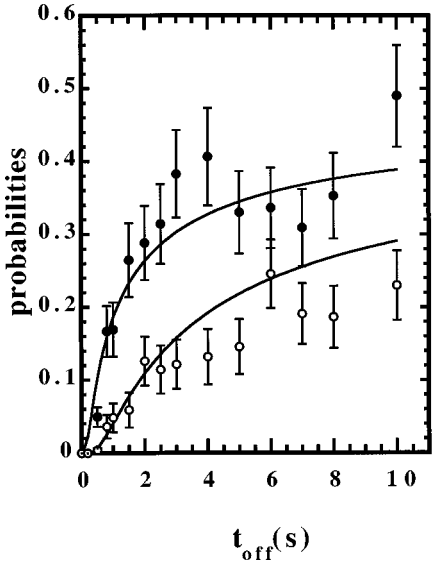

FIG. 6. Probabilities p_f (solid circles) and p_b (open circles) as a function of t_{off} for 0.5-μm CM latex beads on the grating 300/0.36. The solid lines represent the theoretical expressions (1) and (2) with no adjusted parameter.

them in its vicinity [9]. Our device allows us to use light spheres even in the negative dielectrophoresis regime.

MOTION OF THE LATEX BEADS

In Fig. 5 is displayed the plot of the different probabilities for 0.5-μm latex beads as a function of t_{off}. The vertical error bars represent the statistical uncertainty $2\sqrt{N_{\pm i}}/N$.

As expected, the probability p_0 for a particle to stay in the same trap is a decreasing function of t_{off}. The probability p_{+1} first increases with t_{off} and then slowly decreases when t_{off} becomes long enough to have a nonzero probability p_{+2}. Since $p_{+1}>p_{-1}>p_{+2}>p_{-2}>p_{+3}$ the global motion is directed and occurs in the predicted direction.

This fact more clearly appears in Fig. 6, which displays the plots of p_f and p_b as functions of t_{off}. Superimposed on the experimental points the solid lines represent the theoretical expressions (1) and (2). Note that in this case there is no adjustable parameter, the diffusion coefficient and the characteristic lengths of the potential being just plugged into the analytical expressions. Although the dispersion of the experimental points is important, the behavior of the particles is very well described by the simple theoretical laws stated in the first part of this paper. Moreover, although we have calculated the field distribution in the static case (we neglect charge displacements in the bulk of the electrolyte), the description of the potential experienced by the particles is in good agreement with the experimental results.

DIFFERENT SURFACE FUNCTIONS EXHIBIT THE SAME BEHAVIOR

Similar results were obtained with a variety of latex spheres of diameter 0.2 μm, exhibiting different surface groups: Carboxylate-modified, aldehyde sulfate, or sulfate latex spheres had similar behaviors as what is described in the preceding part. Of all the tested surface functions, the amine-modified latex spheres only could not be studied due to a strong sticking of the particles on the grating surface. The carboxyl latex spheres which are much less charged than the CM latex spheres seemed to be insensitive to the field.

MOTION IN REGIMES OF POSITIVE AND NEGATIVE DIELECTROPHORESIS

We have studied the motion of the particles in the regime of positive dielectrophoresis which occurs when the salinity of the solution is not modified by ions leaching from the vacuum grease. These experiments are performed without sealing the cell. Extreme care is then taken to avoid leaks.

Figure 7 displays the plot of the probability p_f as a function of t_{off} for 0.5-μm latex beads. The solid circles correspond to a regime of positive dielectrophoresis, whereas the open ones correspond to a regime of negative dielectrophore-

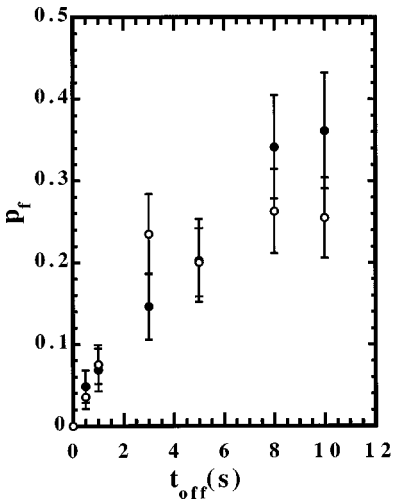

FIG. 7. Probability p_f as a function of t_{off} for 0.5-μm CM latex beads on the grating 150/0.16 in the case of a trapping in the positive (solid circles) and negative (open circles) dielectrophoresis regimes.

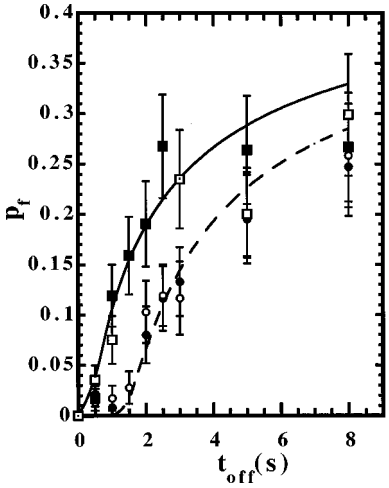

FIG. 8. Probability p_f as a function of t_{off} for different estimated concentrations of 0.5-μm CM latex beads on the grating 150/0.16: $c=0.04\%$ (solid circles), $c=0.02\%$ (open circles), $c=0.01\%$ (solid squares), and $c=0.002\%$ (open squares). At low concentrations, the behavior of the particles is well described by Eq. (1) (solid line), whereas at high concentrations it becomes necessary to plug a latency time as in Eq. (4) (dotted line, $t_1=1$ s).

sis similar to what is described in the preceding part. The regime of positive dielectrophoresis was observed with a frequency of the applied voltage of 100 kHz. Resulting motion is directed towards the left in Fig. 2 in the positive dielectrophoresis regime and towards the right in the negative dielectrophoresis regime. As shown on the plot, the values of the probability p_f are the same within statistical uncertainty in both cases.

The location of trapping changes the direction of motion, but not its absolute value. The energetic potentials deriving from the dielectrophoretic force have therefore the same characteristic distances a and b in both regimes and are inverted one from the other.

INFLUENCE OF THE CONCENTRATION

In all the studied cases, the volume fraction of the particles is of the order of $10^{-2}\%$. As a matter of fact, using the technique reported here, we cannot use much more concentrated solutions since we have to be able to track individual particles. At these concentrations or even at much higher concentrations, we do not expect any effect of the concentration on the diffusion coefficients and thus on the probabilities extracted from our experiments. However, Fig. 8 shows different plots of probabilities p_f for 0.5-μm CM latex beads as a function of t_{off} corresponding to different estimated concentrations. Two different behaviors emerge: At the lowest concentrations (0.01% and 0.002%), p_f is nicely described by the theoretical expression (1), whereas at higher concentrations (0.04% and 0.02% in volume) the probability remains very small at short times and increases only after a time of the order of 2 s.

Although the concentration in the bulk of the cell is too low to have interacting particles in the absence of an external field, this is no longer true when they are trapped. In that case, they are confined to the vicinity of the traps and local concentrations can become very high. When the field is switched off, the free diffusion of the particles is hindered and the distance over which they diffuse dramatically decreases. This is why one observes a much slower increase of p_f vs t_{off} than what is expected. At higher values of t_{off}, this effect is less important since the local concentrations decrease and a more normal diffusive behavior is recovered.

TABLE III. Estimated concentrations in volume of the suspensions of CM latex beads and corresponding latency times obtained by fitting Eq. (4) to the experimental values.

	Latex 0.5 μm	Latex 1 μm	Latex 2 μm	Latex 2.5 μm
Grating 150/0.09	$c=0.04\%$ $t_1=1.5$ s	$c=0.08\%$ $t_1=2.5$ s	$c=0.9\%$ $t_1=10$ s	
Grating 300/0.36	$c=0.01\%$ $t_1=0$	$c=0.05\%$ $t_1=2$ s	$c=0.1\%$ $t_1=3$ s	
Grating 150/0.16	$c=0.002\%$ and $c=0.01\%$ $t_1=0$	$c=0.01\%$ $t_1=2$ s		$c=0.1\%$ $t_1=7$ s
Grating 150/0.16	$c=0.04\%$ and $c=0.02\%$ $t_1=1$ s			

This concentration effect can thus be empirically characterized by a ''latency time'' t_1. In Fig. 8 the experimental values of p_f at higher concentrations are fitted following the equation

$$p_f=\frac{1}{2}\,\text{erfc}\left(\frac{a}{\sqrt{4D(t_{\text{off}}-t_1)}}\right). \tag{4}$$

In that case, with $t_1=1$ s, one recovers a good description of the phenomenon. A similar behavior is observed for each size of latex beads. Table III summarizes these results and gives the value of the latency time in each case.

INFLUENCE OF a AND b

As a and b appear directly in the expressions of p_f and p_b, it is tempting to minimize the ratio $x=a/(a+b)$ characterizing the asymmetry of the potential in order to get a higher drift. The calculation of the field intensity has shown that decreasing the length a_g of the grating also implies a decrease of the length a of the potential, although not to the same extent.

The macroscopic drift is given by

$$J=\sum_{i>0}(ip_{+i}-ip_{-i}). \tag{5}$$

Figure 9 shows the plot of the drift of 1-μm beads as a function of the dimensionless parameters $x=a/(a+b)$ and $d=D^*t_{\text{off}}/(a+b)^2$ characterizing the duration of the diffusion period. Each value of x corresponds to a different grating. These plots are similar in shape to the numerical data of Ref. [1]. They nevertheless exhibit a difference: Whereas the macroscopic drift increases when $x=a/(a+b)$ decreases in Ref. [1], the curve corresponding to $x=0.21$ in Fig. 9 is

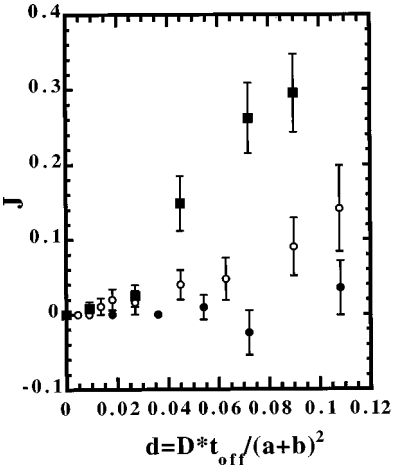

FIG. 9. Macroscopic drift J as a function of the dimensionless parameter $d=D^{*}t_{\mathrm{off}}/(a+b)^{2}$ for 1-μm CM latex beads and for different values of the asymmetry ratio $x=a/(a+b)$: $x=0.34$ (solid circles), $x=0.24$ (solid squares), and $x=0.21$ (open circles).

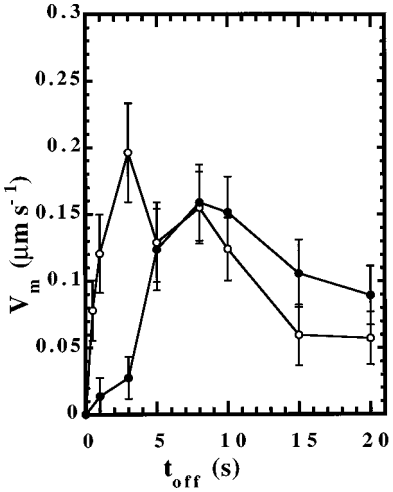

FIG. 10. Measured velocities V_m of 0.5-μm (open circles) and 1-μm (solid circles) CM latex beads on the grating 150/0.16 as a function of t_{off}.

placed between the curves corresponding to $x=0.24$ and $x=0.34$, which means that a smaller asymmetry does not necessarily yield to a larger drift.

As a matter of fact, the calculated lengths a and b of the potential nicely describe the experimental results obtained for the three sizes of beads with the gratings 150/0.16 and 300/0.36, whereas it is not the case for the grating 150/0.09. With this last grating (which corresponds to the smallest calculated asymmetry ratio $x=0.21$), the probabilities p_f and p_b for the 1- and 2-μm beads cannot be described by simply injecting the calculated lengths a and b in Eqs. (1) and (2). By fitting Eqs. (1) and (2) to the experimental values of p_f and p_b corresponding to these plots, it is easy to determine the effective lengths a' and b' ''seen'' by the particles. This is done with respect to the value of the period of the grating $a'+b'=a+b$.

The effective distances a' we obtain by doing so are, respectively, 2.5 and 3.3 μm for 1- and 2-μm beads, which is in both cases far larger than the computed distance $a=1.42$ μm of the potential.

As this deviation from the calculated potential is not observed with the same grating and 0.5-μm beads, we have to invoke steric effects which may be involved in the trapping of 1- and 2-μm beads and which implies that the potential experienced by the beads also depends on their sizes.

MACROSCOPIC VELOCITIES AND SEPARATIONS

The macroscopic velocity of a particle V_m at a given t_{off} is given by

$$V_m=\frac{(a+b)}{(t_{\mathrm{on}}+t_{\mathrm{off}})}\,J. \tag{6}$$

The velocities we have measured correspond to single bead size suspensions and therefore may be obtained for different concentrations. However, as we have shown that the effect of high concentrations can be described by injecting a latency time in the expressions for the probabilities, it is possible to extrapolate the velocities at weak concentrations in order to allow direct comparisons of the velocities. We have therefore shifted each curve by the value of the corresponding latency time and consequently renormalized the velocities such that $V_m=[(a+b)/(t_{\mathrm{on}}+t_{\mathrm{off}}-t_1)]J$ when necessary. All the velocity curves presented hereafter are thus real or extrapolated velocities at small concentrations (zero latency time).

Figure 10 displays the plot of the velocities of two different latex beads as a function of t_{off}. These values are obtained with the grating 150/0.16 and for one single size of beads for each experiment. However, we have checked that the experiment performed with a suspension in which 0.5- and 1-μm beads are both present at a similar concentration gives the same results within the statistical error. The curves displayed in Fig. 10 can therefore be directly compared.

The velocity curves both exhibit maxima, the values of which are rather weak, but the most striking fact is the difference of behaviors according to the size of the beads. For instance, at $t_{\mathrm{off}}=3$ s the 0.5-μm beads move at a speed of 0.2 μm s^{-1}, whereas the 1-μm beads almost move 10 times slower.

The results obtained with two other gratings having different lengths a and b display similar results and in particular a good contrast between the curves corresponding to different sizes of beads.

Figure 11 shows the plot of the velocities as a function of $t_{\mathrm{off}}-t_1$ of 1- and 2-μm particles for the grating 300/0.36. The velocities are smaller than the ones obtained with the grating 150/0.16 due to the high asymmetry ratio of the grating 300/0.36. However, the contrast between the curves is still very good as the 2-μm beads have a zero velocity at the time for which the velocity of the 1-μm beads is maximum.

Finally, Fig. 12 displays the velocities of 0.5- and 1-μm particles on the grating 150/0.09 as a function of $t_{\mathrm{off}}-t_1$. In this case, the fact that the effective distance a' experienced by the particles differ for 0.5- and 1-μm beads improves the separation of the maxima of the velocity curves.

This last result thus shows that the grating and in particular the value of the length a can be optimized according to the sizes of the particles to be separated in order to obtain the higher maximum velocities and selectivity.

It is also worth noting that higher values of velocities can

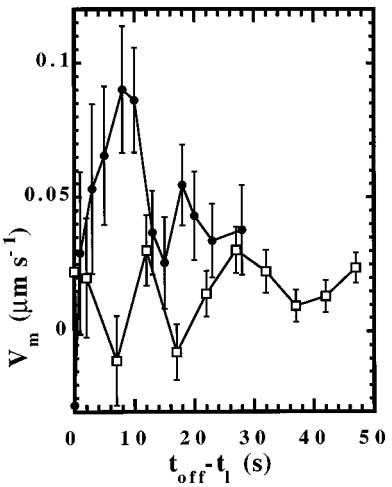

FIG. 11. Extrapolated velocities V_m of 1-μm (solid circles) and 2-μm (open squares) CM latex beads at weak concentration on the grating 300/0.36 as a function of $t_{\mathrm{off}}-t_1$. The negative values of the velocity of the 2-μm beads may be due to a leak.

be reached by reducing the time t_{on} during which the electric field is applied. For practical reasons, we have systematically set $t_{\mathrm{on}}=3$ s, but, as we have pointed out before, a time t_{on} of the order of 0.5 s is enough to obtain an efficient trapping of the particles. The 0.5-μm beads can thus reach a maximal velocity close to 0.35 μm s^{-1} instead of 0.2 μm s^{-1}.

The criterion of the separation of two populations of particles, respectively, moving at velocities V_1 and V_2 with diffusion coefficients D_1 and D_2 is that the maxima of their concentration peaks are separated by a distance equal to the width of the wider concentration peak. The time t^* needed to separate the particles is then given by

$$t^*=\frac{2D_1}{(V_1-V_2)^2}. \tag{7}$$

In our case, the motion of the beads is characterized by their macroscopic velocity V_m and their macroscopic diffusion coefficient D_m [1]:

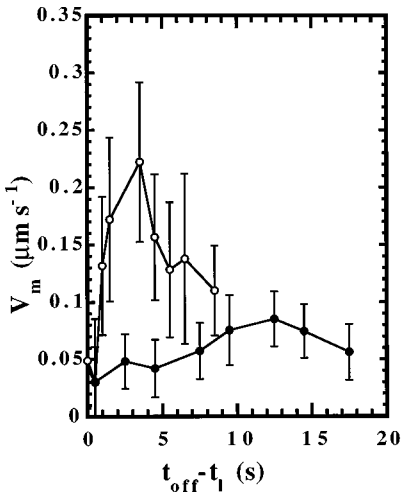

FIG. 12. Extrapolated velocities V_m of 1-μm (solid circles) and 0.5-μm (open circles) CM latex beads on the grating 150/0.09 as a function of $t_{\mathrm{off}}-t_1$.

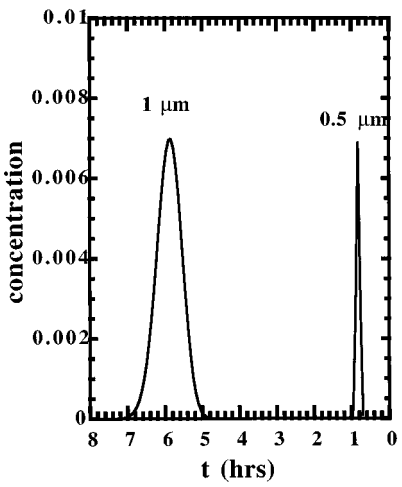

FIG. 13. Expected signal resulting from the separation of 0.5- and 1-μm CM latex beads as a function of time and at a distance $d=1$ mm of the injection on the grating 150/0.16.

$$D_m=(a+b)^2\,\frac{\Sigma_i i^2 p_i-(\Sigma_i i p_i)^2}{2(t_{\mathrm{on}}+t_{\mathrm{off}})}. \tag{8}$$

In any case the values of the macroscopic diffusion coefficients are of the same order as the Brownian diffusion coefficients. For instance, the macroscopic diffusion coefficients calculated from the experimental data of Fig. 10 are, respectively, $D_m=1.13$ and 0.15 μm^2 s^{-1} for 0.5- and 1-μm beads for $t_{\mathrm{on}}=0.5$ s and $t_{\mathrm{off}}=3$ s (whereas their Brownian diffusion coefficients are, respectively, 0.85 and 0.43 μm^2 s^{-1}). According to these values, 0.5- and 1-μm beads can thus be separated in a time $t^*=27$ s, which corresponds to about eight time cycles with $t_{\mathrm{on}}=0.5$ s and $t_{\mathrm{off}}=3$ s. Although this value is a theoretical one as it does not take into account the experimental conditions of a separation (in particular the problem of the injection of the particles), it gives an idea of the selectivity of the device.

Another way to illustrate the separation power of the device is to plot the concentrations at a given distance d of the injection point as a function of time. Figure 13 shows the concentration peaks of 0.5- and 1-μm beads calculated from the experimental data. They correspond to $t_{\mathrm{on}}=0.5$ s and $t_{\mathrm{off}}=3$ s and to a length of the device $d=1$ mm, supposing the injection is punctual. According to Fig. 13, the separation process is quite slow, but strongly selective.

At that point, it is instructive to compare these performances with what can be obtained using other separation techniques. Field flow fractionation (FFF) is classically used to separate colloidal particles [15]. With this method a few minutes are necessary to separate 1- and 2-μm latex beads [16]. However, the drawback of FFF is that steric effects prevent the separation of, for instance, 0.5- and 1-μm beads. The device presented here could therefore supply to the drawbacks of this technique as it is efficient for a wider range of sizes. The required apparatus, moreover, presents the advantage of being much simpler and cheaper than FFF.

CONCLUSION

In conclusion, we have studied the motion of Brownian particles submitted alternatively in time to a flat and a peri-

odic asymmetric potential. The potential is created by using an optical grating as one of the electrodes and derives from a negative dielectrophoretic force. We have shown that the macroscopic drift is directed and well described by the simple equations predicted by theory. We have in particular studied the influence of the size of the particles and the asymmetry of the potential. The strong dependence of the velocity with the size of the particles induces a very high separation power. As the characteristics of the grating can be chosen according to the size of the objects to be separated, our system could provide a separation technique selective for a wide range of particles sizes. We have limited our study to the case of model colloidal particles, but recent experimental results [17] show that many biological objects and in particular DNA molecules are sensitive to a dielectrophoretic force. The application of our device to such biological objects therefore seems very promising.

ACKNOWLEDGMENTS

We thank J. Prost, A. Ajdari, and D. Chatenay for fruitful discussions. We acknowledge Ultimatech for partial funding of this study.

APPENDIX: CROSSOVER FREQUENCY FROM POSITIVE TO NEGATIVE DIELECTROPHORESIS

In order to explain the variation of the crossover frequency with the radius of the particles, we have to consider the expression of the dielectrophoretic force [18] for a spherical particle:

$$\mathbf{F}=2\pi r^3\varepsilon_0\varepsilon_1\mathrm{Re}(f_{\mathrm{CM}})\boldsymbol{\nabla}\cdot\mathbf{E}^2, \tag{A1}$$

where $\mathbf{E}$ is the applied field, r is the radius of the particles, ε_0 is the permittivity of vacuum, ε_l the relative permittivity of the surrounding liquid, and f_{CM} is the Clausius-Mosotti factor. For a homogeneous particle,

$$f_{\mathrm{CM}}=\frac{\tilde{\varepsilon}_p-\tilde{\varepsilon}_l}{\tilde{\varepsilon}_p+2\tilde{\varepsilon}_l}, \tag{A2}$$

where $\tilde{\varepsilon}_p$ and $\tilde{\varepsilon}_l$ are, respectively, the complex permittivities of the particle and surrounding liquid ($\tilde{\varepsilon}=\sigma+i\omega\varepsilon\varepsilon_0$, where ε is the relative permittivity, σ is the conductivity, and ω is the frequency of the field).

Positive or negative dielectrophoresis therefore occurs according to the sign of the real part of the Clausius-Mosotti factor. The crossover frequency can therefore be calculated from

$$\mathrm{Re}(f_{\mathrm{CM}})=0. \tag{A3}$$

One would then expect the crossover frequency to depend only on the bulk conductivities and permittivities of the particle and the liquid. However, this naive description does not correspond to experimental results obtained with colloidal suspensions [19], and one has to take into account the presence of the ionic double layer. The simplest way of doing so is to consider the double layer as a very thin conducting shell of surface conductance λ_s surrounding the suspended particles [18]. This surface conductance is included in the expression for the volume conductance of the particle such that

$$\sigma_p'=\sigma_p+\frac{2\lambda_s}{r}, \tag{A4}$$

where r is the radius of the particles.

By solving Eq. (A3) and replacing the conductivity σ_p by σ_p', one gets an expression for the crossover frequency which now depends on the radius of the particles and which can be written as

$$f_0^2=M_0+\frac{M_1}{r}+\frac{M_2}{r^2}, \tag{A5}$$

where M_0, M_1, and M_2 are functions of the permittivities and conductivities.

Figure 3 shows the plot of the crossover frequency as a function of r. The solid line is a fit of the experimental data according to Eq. (A5) obtained with $\sigma_p=8\ \mu$S/cm, $\sigma_1=7\ \mu$S/cm, $\lambda_s=0.2$ nS, $\varepsilon_p=2$, and $\varepsilon_1=80$. The values of the conductivity and surface conductance of the latex spheres are in good agreement with the ones determined in Ref. [20]. The dielectrophoretic effects occurring in our latex beads suspensions are therefore well described using a rather simple model.

[1] A. Ajdari, C. R. Prost, C. R. Acad. Sci. II **315**, 1635 (1992); A. Ajdari, J. Lewiner, J. Prost, and J. L. Viovy, U.S. Patent No. 5593565, 1997.
[2] J. Prost, J. F. Chauwin, L. Peliti, and A. Ajdari, Phys. Rev. Lett. **72**, 2652 (1994); C. S. Peskin, G. B. Ermentrout, and G. F. Oster, in *Cell Mechanics and Cellular Engineering*, edited by V. C. Mow *et al.* (Springer-Verlag, New York, 1994).
[3] J. F. Chauwin, A. Ajdari, and J. Prost, Europhys. Lett. **27**, 421 (1994).
[4] R. D. Astumian and M. Bier, Phys. Rev. Lett. **72**, 1766 (1994).
[5] R. D. Vale and F. Oosawa, Adv. Biophys. **26**, 97 (1990).
[6] M. Magnasco, Phys. Rev. Lett. **71**, 1477 (1993).
[7] L. Faucheux, L. Bourdieu, P. Kaplan, and A. Libchaber, Phys. Rev. Lett. **74**, 1504 (1995).
[8] J. Rousselet, L. Salomé, A. Ajdari, and J. Prost, Nature (London) **370**, 446 (1994).
[9] L. Faucheux, and A. Libchaber, J. Chem. Soc. Faraday Trans. **91**, 3163 (1995).
[10] N. Felici, C. R. Hebd. Seances Acad. Sci. B **273**, 1004 (1971).
[11] T. Müller *et al.*, Phys. Rev. D **29**, 340 (1996).

[12] R. Pethig, Y. Huang, X. Wang, and J. Burt, Phys. Rev. D **24**, 881 (1992).
[13] G. Fuhr (private communication).
[14] G. Bruhat, *Electricité* (Masson, Paris, 1959).
[15] J. Calvin Giddings, Science **260**, 1456 (1993).
[16] S. Kim Ratanathanawongs and J. Calvin Giddings, Anal. Chem. **64**, 6 (1992).
[17] M. Washizu, T. Nanba, and S. Masuda, IEEE Trans. Ind. Appl. **26**, 352 (1990); M. Washizu, O. Kurosawa, I. Arai, S. Suzuki, and N. Shimamoto, *ibid.* **31**, 447 (1995).
[18] Herbert A. Pohl, *Dielectrophoresis* (Cambridge University Press, Cambridge, England, 1978).
[19] H. P. Schwan, G. Schwarz, J. Maczuk, and H. Pauly, J. Phys. Chem. **66**, 2626 (1962).
[20] W. M. Arnold, H. P. Schwan, and U. Zimmermann, J. Phys. Chem. **91**, 5093 (1987).